Meccanica (2011) 46:1267–1281
DOI 10.1007/s11012-010-9383-z

Dynamic basic displacement functions in free vibration analysis of centrifugally stiffened tapered beams; a mechanical solution

Reza Attarnejad · Ahmad Shahba

Received: 29 July 2009 / Accepted: 13 November 2010 / Published online: 30 November 2010

Abstract This paper deals with enhancing the existing Finite Element formulations through employing basic principles of structural mechanics accompanied with mathematical techniques. Introducing the concept of Basic Displacement Functions (BDFs), the free vibration analysis of rotating tapered beams is studied from a mechanical point of view. It is shown that exact shape functions could be derived in terms of BDFs. The new shape functions turn out to be dependent on the rotational speed, circular frequency, the position of element along the beam and variation of cross-sectional dimensions along the element. Dynamic BDFs are obtained by applying Adomian Modified Decomposition Method (AMDM) to the governing differential equation of motion. Carrying out numerical examples, the competency of the method is verified.

Keywords Basic displacement functions · Rotating tapered beam · Shape functions · Free vibration · Adomian modified decomposition method

R. Attarnejad · A. Shahba (✉)
School of Civil Engineering, University College of Engineering, University of Tehran, Tehran 11365-4563, Iran
e-mail: shahba@ut.ac.ir

A. Shahba
e-mail: ah.shahba@gmail.com

Nomenclature

$A(x)$	cross-sectional area at distance x
A_0	cross-sectional area at $x = 0$
$\mathbf{b}$	vector of BDFs
E	modulus of elasticity
$\mathbf{F}$	vector of nodal forces
$\mathbf{F_{II}}, \mathbf{F_{JJ}}$	nodal flexibility matrices of the left and right nodes respectively
$\mathbf{G}$	matrix containing nodal stiffness matrices
$I(x)$	moment of inertia at distance x
I_0	moment of inertia at $x = 0$
$\mathbf{K}$	flexural stiffness matrix
$\mathbf{K_G}$	geometric stiffness matrix
$\mathbf{K_{II}}, \mathbf{K_{JJ}}$	nodal stiffness matrices of the left and right nodes respectively
L	length of the beam
l_e	length of the element
M	bending moment
$\mathbf{M}$	consistent mass matrix
$\mathbf{N}$	vector of shape functions
q	external transverse load
R	hub radius
t	time
T	centrifugal force
V	shear force
w	transverse displacement
x	longitudinal coordinate along whole beam
$\bar{x}$	longitudinal coordinate along beam element
δ	hub radius parameter
η	non-dimensional rotational speed
θ	angle of rotation

μ	non-dimensional natural frequency
ρ	mass density
ω	circular frequency
Ω	rotational speed

1 Introduction

Rotating beams are mostly encountered in structures designed for mechanical and aerospace intensions such as windmills, helicopter rotor blades and spacecrafts with flexible appendages [1–3]. Due to the presence of centrifugal force and its stiffening effect, the vibration characteristics of the rotating beams, a crucial point in design of rotary machineries, differ significantly from that of non-rotating beams.

The presence of variable coefficients in the governing differential equation for out-of-plane bending vibration of rotating tapered beams, brought up due to the varying centrifugal force and cross-sectional dimensions along beam element, leads to the fact that there is no closed-form solution for this engineering problem; thus numerical techniques such as finite element method [4–12], spectrally formulated finite element method [13, 14], Galerkin method [15, 16], Frobenius series solution [17, 18] and differential transform method [19–23] have been considerably used.

One of the methods which have remarkably attracted attention from the researchers is dynamic stiffness method [24–26] which enables one to exactly determine as many natural frequencies and mode shapes as required with just one element. Banerjee et al. [25] derived the dynamic stiffness matrix for rotating Euler-Bernoulli beams whose cross-sectional area and moment of inertia vary along beam with arbitrary integer power n and $n+2$, respectively.

Assuming the transverse displacement to vary as a fourth order function, Gunda and Ganguli [27] derived rational shape functions which unlike the cubic Hermite shape functions satisfy the static part of the homogeneous governing differential equation of rotating Euler-Bernoulli beams. Recently Gunda et al. [28] have derived new hybrid stiff-string-polynomial functions for vibration analysis of high speed rotating tapered beams. These functions are linear combination of the solution of the governing static differential equation of a stiff-string and a cubic polynomial.

In the present paper, new functions holding structural interpretations, Basic Displacement Functions (BDFs), are introduced from which exact shape functions are derived. Applying AMDM on the out-of-plane bending motion of rotating beams and imposing appropriate boundary conditions, BDFs are obtained on the basis of dynamic deformations. The present method considers the variation of cross-sectional area, moment of inertia and centrifugal force along the element in order to obtain shape functions. The present formulation poses no restriction on the type of functions which describe the variation of cross-sectional area and moment of inertia; hence it is capable of handling a big class of arbitrarily varying beams. The efficiency of the idea of BDFs has been verified for different engineering problems. BDFs are categorized into static BDFs [29–32] and dynamic BDFs [33]. Here the dynamic BDFs are introduced and employed in free vibration analysis.

There are two important questions need to be answered; firstly why do we resort to Finite Element method? Secondly why do we try to enhance Finite Element method? About the first question, we can say that Finite Element method in comparison with other methods is much simpler and more flexible in treating different types of engineering problems with different conditions like dampers, spring-mass systems and abrupt profile changes. About the second question, as previously stated, the cubic Hermite shape functions do not satisfy the governing differential equation of rotating beams. Finite Element method is a displacement-based method (stiffness method) which is established on a prescribed displacement field; that is, an additional hypothesis is imposed apart from the three essential relations namely equilibrium of forces, compatibility of displacements and/or strains and the constitutional law of the material behavior. Due to this extra hypothesis, usually one of the three essential relations is satisfied only in certain interior points of the domain; however application of stiffness method is simple. Unlike the stiffness method, application of the flexibility-based method ensures the exact satisfaction of the equilibrium equations at any interior point of the element; nevertheless its application in engineering problems has mostly been limited to simple ones due to its cumbersome procedures. In this paper, a novel method is proposed which captures its accuracy and exactness from its flexibility basis and its simple application from stiffness method.

2 Basic displacement functions

Basic Displacement Functions (BDFs) are not merely mathematical functions while they hold pure mechanical interpretations. In what follows, BDFs are firstly defined and then it is shown how the shape functions could be obtained in terms of BDFs.

2.1 BDFs definition

BDFs are basically interpreted as the nodal displacements, either transverse displacement or angle of rotation, due to a unit load on the element. BDFs can be defined in detail as

b_{w1}: Transverse displacement of the left node due to an arbitrarily varying axial load and a unit load at distance $\bar{x}$ as shown in Fig. 1a.

$b_{\theta 1}$: Bending rotation of the left node due to an arbitrarily varying axial load and a unit load at distance $\bar{x}$ as shown in Fig. 1b.

b_{w2}: Transverse displacement of the right node due to an arbitrarily varying axial load and a unit load at distance $\bar{x}$ as shown in Fig. 1c.

$b_{\theta 2}$: Bending rotation of the right node due to an arbitrarily varying axial load and a unit load at distance $\bar{x}$ as shown in Fig. 1d.

On the basis of reciprocal theorem, an equivalent system is considered for each BDF; that is, an equivalent definition is presented for BDFs which states that BDFs are the transverse displacement of an arbitrary point on the element due to a unit nodal load, either lateral load or moment. The equivalent definitions of BDFs are defined in detail as

b_{w1}: Transverse displacement at distance $\bar{x}$ due to an arbitrarily varying axial load and a unit load at the left node of a free-clamped beam as shown in Fig. 2a.

$b_{\theta 1}$: Transverse displacement at distance $\bar{x}$ due to an arbitrarily varying axial load and a unit moment at the left node of a free-clamped beam as shown in Fig. 2b.

b_{w2}: Transverse displacement at distance $\bar{x}$ due to an arbitrarily varying axial load and a unit load at the right node of a clamped-free beam as shown in Fig. 2c.

$b_{\theta 2}$: Transverse displacement at distance $\bar{x}$ due to an arbitrarily varying axial load and a unit moment at the right node of a clamped-free beam as shown in Fig. 2d.

The definitions of nodal flexibilities for a beam under axial loading are shown in Fig. 3. Comparing Fig. 3 with the equivalent definition of BDFs in Fig. 2, one can evaluate the nodal flexibility matrices in terms of BDFs as

$$\mathbf{F_{II}} = \begin{bmatrix} b_{w1}(0) & b_{\theta 1}(0) \\ \frac{db_{w1}}{d\bar{x}}|_{\bar{x}=0} & \frac{db_{\theta 1}}{d\bar{x}}|_{\bar{x}=0} \end{bmatrix} \tag{1}$$

$$\mathbf{F_{JJ}} = \begin{bmatrix} b_{w2}(l_e) & b_{\theta 2}(l_e) \\ \frac{db_{w2}}{d\bar{x}}|_{\bar{x}=l_e} & \frac{db_{\theta 2}}{d\bar{x}}|_{\bar{x}=l_e} \end{bmatrix} \tag{2}$$

where points I and J are respectively the left and right nodes of the element. Once inverting nodal flex-

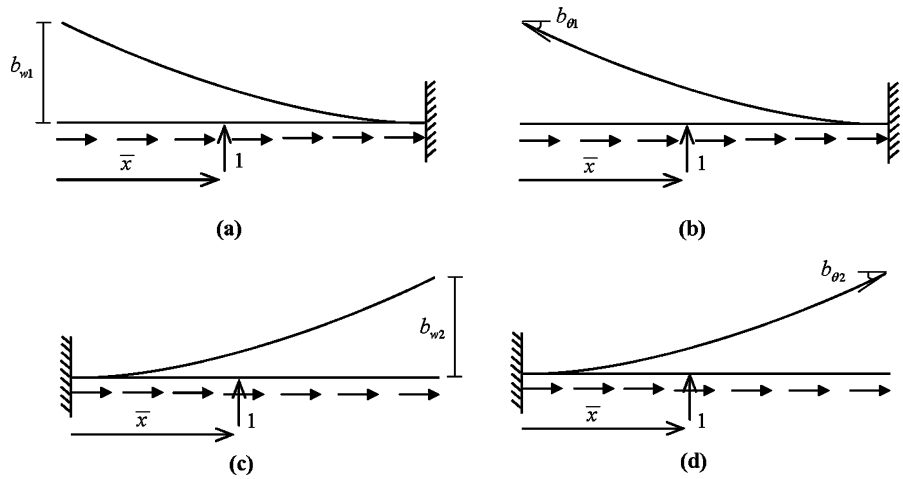

Fig. 1 Definitions of (**a**) b_{w1}; (**b**) $b_{\theta 1}$; (**c**) b_{w2} and (**d**) $b_{\theta 2}$

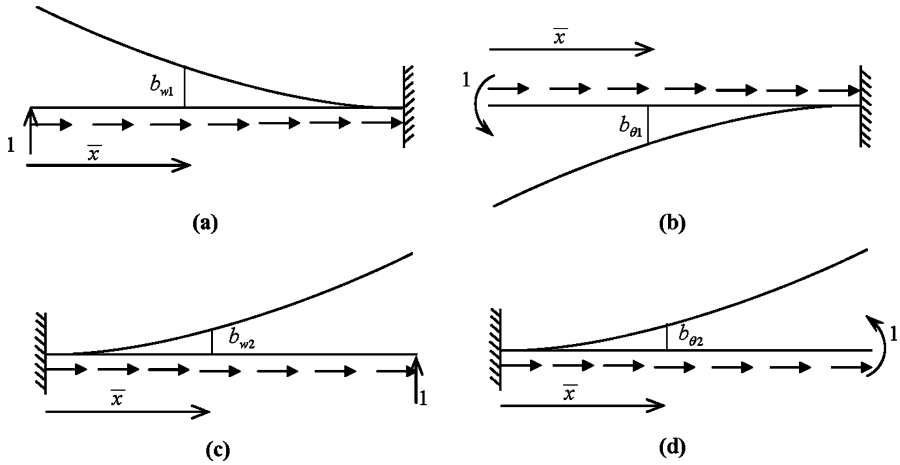

Fig. 2 Equivalent definitions of (**a**) b_{w1}; (**b**) $b_{\theta 1}$; (**c**) b_{w2} and (**d**) $b_{\theta 2}$

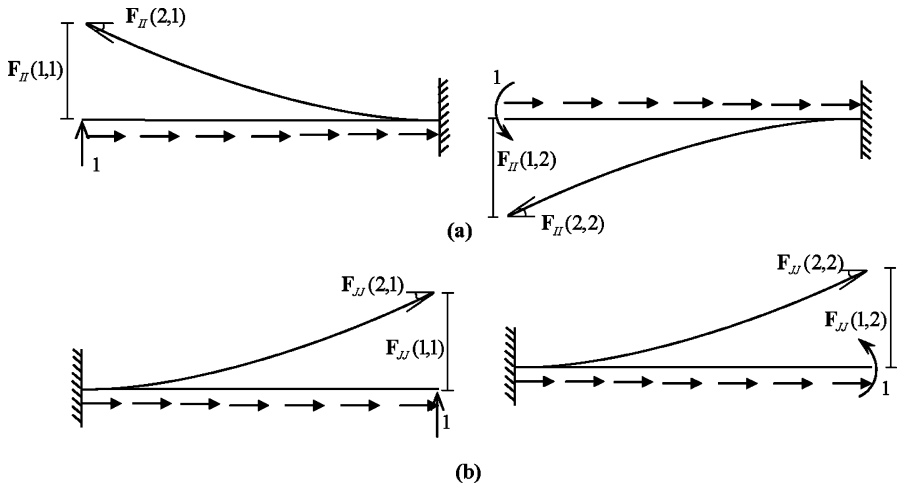

Fig. 3 Illustration of nodal flexibilities of (**a**) left node; (**b**) right node

ibility matrices, the nodal stiffness matrices are evaluated.

2.2 Shape functions

A schematic of a non-prismatic beam element is shown in Fig. 4. The system has to be decomposed into two isostatic systems i.e. cantilever beams in order to calculate the support reactions. Looking deeply, the nodal displacements of point (J) in Fig. 4b can be expressed in terms of BDFs as,

$$\begin{Bmatrix} w_J \\ \theta_J \end{Bmatrix}^{(b)} = \int_0^{l_e} q(\bar{x}) \begin{Bmatrix} b_{w2} \\ b_{\theta 2} \end{Bmatrix} d\bar{x} \tag{3}$$

The nodal displacements of point (J) in Fig. 4c are given as

$$\begin{Bmatrix} w_J \\ \theta_J \end{Bmatrix}^{(c)} = \mathbf{F_{JJ}} \begin{Bmatrix} V_J \\ M_J \end{Bmatrix} \tag{4}$$

where $\mathbf{F_{JJ}}$ is the nodal flexibility of point (J) given in (1). Following superposition principle, we have

$$\begin{Bmatrix} w_J \\ \theta_J \end{Bmatrix}^{(a)} = \begin{Bmatrix} w_J \\ \theta_J \end{Bmatrix}^{(b)} + \begin{Bmatrix} w_J \\ \theta_J \end{Bmatrix}^{(c)} = \mathbf{0} \tag{5}$$

and using (3) and (4), one obtains

$$\begin{Bmatrix} V_J \\ M_J \end{Bmatrix} = -\mathbf{K_{JJ}} \int_0^{l_e} q(\bar{x}) \begin{Bmatrix} b_{w2} \\ b_{\theta 2} \end{Bmatrix} d\bar{x} \tag{6}$$

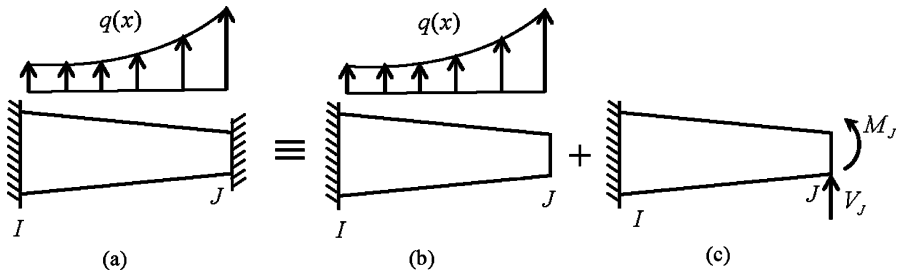

Fig. 4 General non-prismatic beam decomposed into isostatic structures

in which $\mathbf{K_{JJ}}$ is the nodal stiffness of point (J). Similarly the support reactions at point (I) are obtained as

$$\begin{Bmatrix} V_I \\ M_I \end{Bmatrix} = -\mathbf{K_{II}} \int_0^{l_e} q(\bar{x}) \begin{Bmatrix} b_{w1} \\ b_{\theta 1} \end{Bmatrix} d\bar{x} \tag{7}$$

Knowing that the nodal equivalent forces are the opposite of support reactions; (6) and (7) are written in matrix form as

$$\mathbf{F} = \mathbf{G} \int_0^{l_e} q(\bar{x}) \mathbf{b} d\bar{x} \tag{8}$$

in which $\mathbf{b} = \{b_{w1}\ b_{\theta 1}\ b_{w2}\ b_{\theta 2}\}^T$ and

$$\mathbf{G} = \begin{bmatrix} \mathbf{K_{II}} & \mathbf{0} \\ \mathbf{0} & \mathbf{K_{JJ}} \end{bmatrix} \tag{9}$$

According to the Finite Element method, the nodal equivalent forces and the structural matrices are given as

$$\mathbf{F} = \int_0^{l_e} q(\bar{x}) \mathbf{N}^T d\bar{x} \tag{10}$$

$$\mathbf{M} = \int_0^{l_e} \mathbf{N}^T \rho A(\bar{x}) \mathbf{N} d\bar{x} \tag{11}$$

$$\mathbf{K_G} = \int_0^{l_e} \mathbf{N'}^T T(\bar{x}) \mathbf{N'} d\bar{x} \tag{12}$$

$$\mathbf{K} = \int_0^{l_e} \mathbf{N''}^T E I(\bar{x}) \mathbf{N''} d\bar{x} \tag{13}$$

Comparing (8) and (10), the new shape functions are derived as

$$\mathbf{N} = \mathbf{b}^T \mathbf{G} \tag{14}$$

therefore the structural matrices i.e. consistent mass, geometric stiffness and flexural stiffness are respectively given as

$$\mathbf{M} = \mathbf{G} \left(\int_0^{l_e} \mathbf{b} \rho A(\bar{x}) \mathbf{b}^T d\bar{x} \right) \mathbf{G} \tag{15}$$

$$\mathbf{K_G} = \mathbf{G} \left(\int_0^{l_e} \mathbf{b'} T(\bar{x}) \mathbf{b'}^T d\bar{x} \right) \mathbf{G} \tag{16}$$

$$\mathbf{K} = \mathbf{G} \left(\int_0^{l_e} \mathbf{b''} E I(\bar{x}) \mathbf{b''}^T d\bar{x} \right) \mathbf{G} \tag{17}$$

It is expected that the new shape functions show high accuracy in dynamic analysis of rotating tapered beams since they have been obtained in terms of BDFs where it will be shown that in their computations many system parameters are taken into consideration including variation of area and moment of inertia along element axis, circular frequency and centrifugal force which by itself is dependent on the position of the element along the beam, hub radius and the rotational speed.

3 Computation of BDFs

A schematic of a non-prismatic rotating beam is illustrated in Fig. 5. The governing differential equation for out-of-plane bending motion of rotating tapered beams is given by

$$\frac{\partial^2}{\partial \bar{x}^2} \left(E I(\bar{x}) . \frac{\partial^2 W}{\partial \bar{x}^2} \right) + \rho A(\bar{x}) . \frac{\partial^2 W}{\partial t^2} - \frac{\partial}{\partial \bar{x}} \left(T(\bar{x}) . \frac{\partial W}{\partial \bar{x}} \right) = q(\bar{x}, t) \tag{18}$$

where the centrifugal force in the ith element is given as

$$T(\bar{x}) = \int_{x_i + \bar{x}}^{L} \rho A(x) . \Omega^2 . (R + x) . dx \tag{19}$$

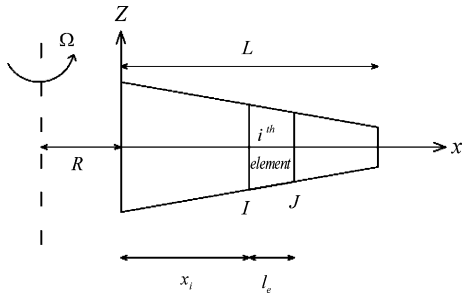

Fig. 5 Rotating tapered beam configuration

According to the equivalent definition of BDFs, BDFs are transverse displacement W of any point on the element due to a unit nodal load; that is, one can compute BDFs by solving (18) for $q(x,t)=0$. Moreover, assuming a sinusoidal variation of transverse displacement with circular frequency ω, (18) is written as

$$\frac{d^2}{d\bar{x}^2}\left(EI\frac{d^2w}{d\bar{x}^2}\right)-\omega^2\rho Aw - \frac{d}{d\bar{x}}\left(T(\bar{x})\frac{dw}{d\bar{x}}\right)=0 \tag{20}$$

As previously mentioned, numerical methods have to be employed to solve (20). In this paper, we employ AMDM which is an efficient technique for solution of both ordinary and partial differential equations. In what follows, we briefly introduce the concept of AMDM and then it is shown how it could be used to solve the governing differential equation.

3.1 Adomain modified decomposition method

Consider a general ordinary differential equation as

$$\mathbf{L}y+\mathbf{R}y+\mathbf{N}y=g(x) \tag{21}$$

in which $\mathbf{L}$ is an invertible linear operator taken as the highest-order derivative; $\mathbf{R}$ is the remainder of the linear operator and $\mathbf{N}$ is the nonlinear operator. Solving (21) for $\mathbf{L}y$, we have

$$y=\Phi+\mathbf{L}^{-1}g-\mathbf{L}^{-1}\mathbf{R}y-\mathbf{L}^{-1}\mathbf{N}y \tag{22}$$

where Φ is the integration constant and $\mathbf{L}\Phi=0$. In order to solve (21) by AMDM, y, $g(x)$ and $\mathbf{N}y$ are represented by infinite series as [34]

$$\begin{aligned} &y(x)=\sum_{i=0}^{\infty}c_ix^i, \qquad g(x)=\sum_{i=0}^{\infty}g_ix^i \\ &\mathbf{N}y=\sum_{i=0}^{\infty}A_i(c_0,c_1,\ldots,c_i)x^i \end{aligned} \tag{23}$$

in which A_i are Adomian coefficients. Substituting (23) into (22), we have

$$\begin{aligned} y=\sum_{i=0}^{\infty}c_ix^i=\Phi&+\mathbf{L}^{-1}\left(\sum_{i=0}^{\infty}g_ix^i\right) \\ &-\mathbf{L}^{-1}\mathbf{R}\left(\sum_{i=0}^{\infty}c_ix^i\right) \\ &-\mathbf{L}^{-1}\left(\sum_{i=0}^{\infty}A_i(c_0,c_1,\ldots,c_i)x^i\right) \end{aligned} \tag{24}$$

The coefficients c_i can be computed by the recurrence relation. In practical applications, the infinite series is replaced by an approximate truncated series $\sum_{i=0}^{n-1}c_ix^i$ with n terms.

3.2 BDFs computation

Expanding (20) and using the dimensionless parameter $\xi=x/l_e$, the following relation is obtained.

$$W''''+A(\xi)W'''+B(\xi)W''+C(\xi)W' + D(\xi)W=0 \tag{25}$$

in which

$$\begin{aligned} A(\xi)&=2EI'(\xi)/EI(\xi) \\ B(\xi)&=[EI''(\xi)-l_e^2T(\xi)]/EI(\xi) \\ C(\xi)&=-l_e^2T'(\xi)/EI(\xi) \\ D(\xi)&=-\omega^2l_e^4\rho A(\xi)/EI(\xi) \end{aligned} \tag{26}$$

Using power series expansion, the coefficients in the differential (25) are expressed as

$$A(\xi)=\sum_{k=0}^{\infty}a_k\xi^k,\qquad B(\xi)=\sum_{k=0}^{\infty}b_k\xi^k$$
$$C(\xi)=\sum_{k=0}^{\infty}c_k\xi^k,\qquad D(\xi)=\sum_{k=0}^{\infty}d_k\xi^k \tag{27}$$

Employing AMDM on (25), we have

$$W=\Phi-\mathbf{L}^{-1}[A(\xi)W'''+B(\xi)W''+C(\xi)W' + D(\xi)W] \tag{28}$$

where $\mathbf{L}^{-1}=\int_0^{\xi}\int_0^{\xi}\int_0^{\xi}\int_0^{\xi}\cdots d\xi d\xi d\xi d\xi$ and $\Phi=\sum_{k=0}^{3}\frac{d^kW}{d\xi^k}|_{\xi=0}\xi^k$. Moreover using Cauchy product we obtain

$$D(\xi)W=\sum_{k=0}^{\infty}d_k\xi^k\times\sum_{k=0}^{\infty}w_k\xi^k=\sum_{k=0}^{\infty}\xi^k\sum_{j=0}^{k}d_{k-j}w_j$$
$$C(\bar{x})W'=\sum_{k=0}^{\infty}c_k\xi^k\times\sum_{k=0}^{\infty}(k+1)w_{k+1}\xi^k =\sum_{k=0}^{\infty}\xi^k\sum_{j=0}^{k}(j+1)c_{k-j}w_{j+1} \tag{29}$$
$$B(\xi)W''=\sum_{k=0}^{\infty}\xi^k\sum_{j=0}^{k}(j+1)(j+2)b_{k-j}w_{j+2}$$
$$A(\xi)W'''=\sum_{k=0}^{\infty}\xi^k\sum_{j=0}^{k}(j+1)(j+2)(j+3)a_{k-j}w_{j+3}$$

Once substituting (29) into (28) and integrating four times, we obtain

$$W=\sum_{k=0}^{\infty}w_k\xi^k=\Phi-\sum_{k=0}^{\infty}\frac{(k!)\xi^{k+4}}{(k+4)!} \times\sum_{j=0}^{k}[(j+1)(j+2)(j+3)a_{k-j}w_{j+3} +(j+1)(j+2)b_{k-j}w_{j+2} +(j+1)c_{k-j}w_{j+1}+d_{k-j}w_j] \tag{30}$$

The following recurrence relations are obtained by equating the coefficients of the like powers of ξ in (30).

- For $0\le k\le 3$:

$$w_k=\left.\frac{d^kW}{d\xi^k}\right|_{\xi=0}$$

- For $k\ge 4$:

$$w_k=-\frac{(k-4)!}{k!}\sum_{j=0}^{k-4}[(j+1)(j+2) \times(j+3)a_{k-j-4}w_{j+3} +(j+1)(j+2)b_{k-j-4}w_{j+2} +(j+1)c_{k-j-4}w_{j+1}+d_{k-j-4}w_j] \tag{31}$$

At this stage the problem reduces to determination of the first four terms of $W(\xi)$ which requires imposing the boundary conditions for each BDF. On the basis of the equivalent definitions of BDFs shown in Fig. 2, the boundary conditions for BDFs read as

$$b_{w1}:\quad V|_{\xi=0}=1,\quad M|_{\xi=0}=0,\quad W|_{\xi=1}=0,\quad \theta|_{\xi=1}=0 \tag{32a}$$
$$b_{\theta1}:\quad V|_{\xi=0}=0,\quad M|_{\xi=0}=-1,\quad W|_{\xi=1}=0,\quad \theta|_{\xi=1}=0 \tag{32b}$$
$$b_{w2}:\quad W|_{\xi=0}=0,\quad \theta|_{\xi=0}=0,\quad V|_{\xi=1}=-1,\quad M|_{\xi=1}=0 \tag{32c}$$
$$b_{\theta2}:\quad W|_{\xi=0}=0,\quad \theta|_{\xi=0}=0,\quad V|_{\xi=1}=0,\quad M|_{\xi=1}=1 \tag{32d}$$

From the Euler-Bernoulli beam theory, angle of rotation, bending moments and shear forces are respectively given as

$$\theta(\xi)=\frac{1}{l_e}\frac{dW}{d\xi} \tag{33a}$$
$$M(\xi)=\frac{EI(\xi)}{l_e^2}\frac{d^2W}{d\xi^2} \tag{33b}$$
$$V(\xi)=\frac{1}{l_e^3}\frac{d}{d\xi}\left(EI(\xi)\frac{d^2W}{d\xi^2}\right)-\frac{T(\xi)}{l_e}\frac{dW}{d\xi} \tag{33c}$$

Using (32) and (33), BDFs are obtained as polynomials. The following procedure is proposed to derive new shape functions using BDFs.

(a) Derivation of BDFs using Sect. 3.2.

Table 1 Dimensionless natural frequencies for different combinations of height c_h and breadth c_b taper ratios

c_b	c_h					
	0		0.3		0.6	
	Present	Downs [36]	Present	Downs [36]	Present	Downs [36]
First mode						
0	3.51601	3.51602	3.66675	3.66675	3.93428	3.93428
0.3	3.91602	3.91603	4.06693	4.06693	4.33622	4.33622
0.6	4.58530	4.58531	4.73720	4.73721	5.00903	5.00903
0.8	5.39758	5.39759	5.55296	5.55297	5.82882	5.82882
Second mode						
0	22.0345	22.0345	19.8806	19.8806	17.4878	17.4879
0.3	22.7859	22.7860	20.5555	20.5555	18.0803	18.0803
0.6	24.0211	24.0211	21.6698	21.6699	19.0649	19.0649
0.8	25.6558	25.6558	23.1578	23.1578	20.3952	20.3952
Third mode						
0	61.6972	61.6972	53.3222	53.3222	44.0248	44.0248
0.3	62.4361	62.4361	54.0152	54.0152	44.6583	44.6583
0.6	63.7515	63.7515	55.2224	55.2224	45.7384	45.7384
0.8	65.7470	65.7470	57.0156	57.0157	47.3051	47.3051
Fourth mode						
0	120.902	120.902	103.267	103.267	83.5541	83.5541
0.3	121.648	121.648	103.975	103.975	84.2100	84.2101
0.6	123.025	123.025	105.241	105.241	85.3438	85.3438
0.8	125.264	125.264	107.231	107.231	87.0561	87.0561

Table 2 Dimensionless natural frequencies under different rotational speed parameters

η	First mode		Second mode		Third mode	
	Present	Ref. [27]	Present	Ref. [27]	Present	Ref. [27]
0	3.8238	3.8239	18.3173	18.3173	47.2648	47.2649
1	3.9866	3.9866	18.4740	18.4740	47.4173	47.4173
2	4.4368	4.4368	18.9366	18.9366	47.8716	47.8717
3	5.0927	5.0927	19.6839	19.6839	48.6190	48.6190
4	5.8788	5.8788	20.6851	20.6852	49.6456	49.6457
5	6.7434	6.7434	21.9053	21.9053	50.9338	50.9339
6	7.6551	7.6551	23.3093	23.3093	52.4633	52.4633
7	8.5956	8.5956	24.8647	24.8647	54.2124	54.2125
8	9.5539	9.5540	26.5436	26.5437	56.1595	56.1596
9	10.5239	10.5239	28.3227	28.3227	58.2833	58.2834
10	11.5015	11.5016	30.1827	30.1828	60.5639	60.5640
11	12.4845	12.4845	32.1085	32.1086	62.9829	62.9830
12	13.4711	13.4711	34.0877	34.0877	65.5236	65.5238

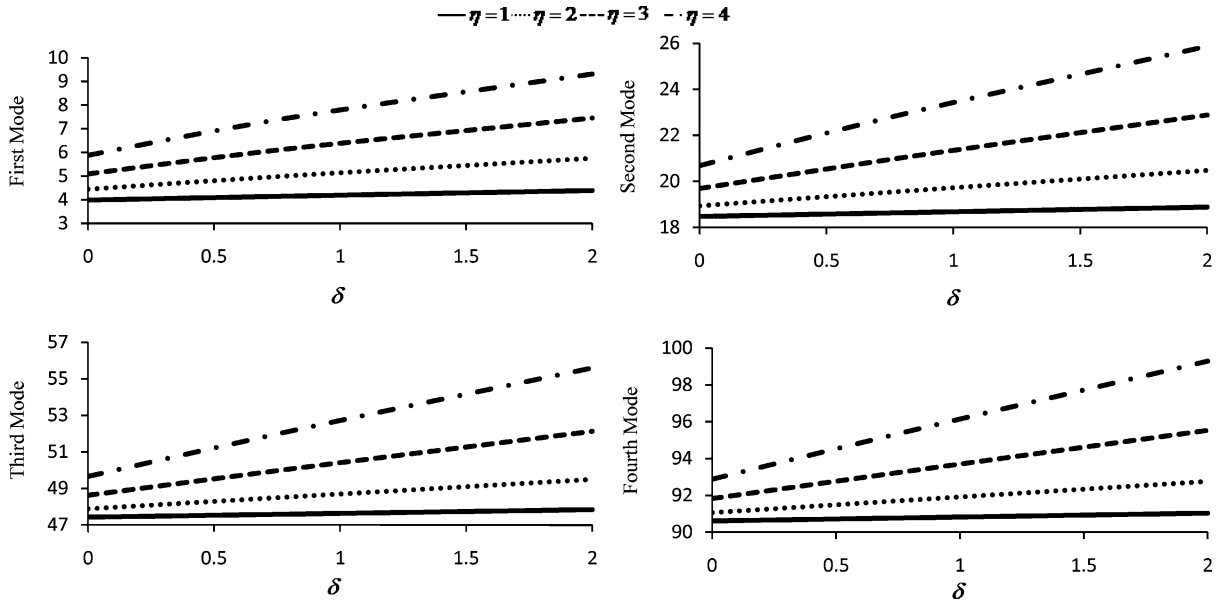

Fig. 6 Variation of natural frequencies with respect to hub radius parameter for different rotational speed parameters

(b) Evaluating nodal flexibility matrices using (1) and (2).
(c) Evaluating structural matrices using (15)–(17).

4 Numerical results

Obtaining the structural matrices, free vibration analysis is carried out by general eigenvalue analysis [35],

$$(\mathbf{K}+\mathbf{K_G})\phi=\omega^2\mathbf{M}\phi \tag{34}$$

in which ω is the natural frequency. The following dimensionless parameters are introduced to present the numerical results.

$$\delta=\frac{R}{L},\qquad \eta=\Omega\sqrt{\frac{\rho A_0L^4}{EI_0}}$$
$$\mu=\omega\sqrt{\frac{\rho A_0L^4}{EI_0}} \tag{35}$$

In what follows, four numerical examples are provided including non-rotating double tapered beam, rotating beam with linearly varying height, rotating double tapered beam with equal height and breadth taper ratios and non-rotating stepped beam. In Examples 1–3, free vibration analysis in carried out for cantilever boundary conditions due to its wide application in engineering problems and well coverage in the literature.

4.1 Example 1: non-rotating double-tapered beam

A non-rotating double tapered beam with rectangular cross-section whose height and breadth both vary linearly is considered. The first four dimensionless frequencies for different combinations of height and breadth taper ratios, respectively c_h and c_b, are determined and compared with Downs [36] in Table 1.

4.2 Example 2: linear cross-sectional area and cubic moment of inertia

It is assumed that cross-sectional area and moment of inertia vary as

$$A(x)=A_0\left(1-0.5\frac{x}{L}\right)$$
$$I(x)=I_0\left(1-0.5\frac{x}{L}\right)^3 \tag{36}$$

The first three natural frequencies of the beam with $\delta=0$ for different rotational speed parameters are determined and tabulated in Table 2. The effect of rub radius on the first four natural frequencies of the beam under different rotational speed parameters is investigated in Fig. 6.

Table 3 Dimensionless natural frequencies under different rotational speed parameters; Modes: 1–3

η	First mode		Second mode		Third mode	
	Present	Ref. [25]	Present	Ref. [25]	Present	Ref. [25]
0	4.62514	4.62515	19.5476	19.5476	48.5789	48.5789
1	4.76404	4.76405	19.6803	19.6803	48.7073	48.7073
2	5.15641	5.15641	20.0733	20.0733	49.0906	49.0906
3	5.74577	5.74578	20.7121	20.7121	49.7226	49.7227
4	6.47261	6.47262	21.5749	21.5749	50.5939	50.5938
5	7.29013	7.29014	22.6360	22.6360	51.6918	51.6918
6	8.16628	8.16630	23.8684	23.8684	53.0019	53.0018
7	9.08034	9.08036	25.2461	25.2461	54.5081	54.5082
8	10.0192	10.0192	26.7454	26.7454	56.1941	56.1941
9	10.9747	10.9747	28.3459	28.3459	58.0433	58.0434
10	11.9415	11.9415	30.0299	30.0299	60.0399	60.0399

Table 4 The same as Table 3; Modes: 4–5

η	Fourth mode		Fifth mode	
	Present	Ref. [25]	Present	Ref. [25]
0	91.8128	91.8128	149.3899	149.390
1	91.9409	91.9409	149.5183	149.518
2	92.3243	92.3243	149.9030	149.903
3	92.9597	92.9597	150.5417	150.542
4	93.8415	93.8415	151.4311	151.431
5	94.9626	94.9627	152.5666	152.567
6	96.3142	96.3142	153.9423	153.942
7	97.8861	97.8861	155.5516	155.552
8	99.6672	99.6673	157.3867	157.387
9	101.6458	101.646	159.4393	159.439
10	103.8098	103.810	161.7006	161.701

4.3 Example 3: parabolic cross-sectional area and fourth order moment of inertia

It is assumed that cross-sectional area and moment of inertia vary as

$$A(x) = A_0\left(1 - 0.5\frac{x}{L}\right)^2$$
$$I(x) = I_0\left(1 - 0.5\frac{x}{L}\right)^4 \tag{37}$$

The first five natural frequencies of the beam with $\delta = 0$ are determined and compared with those of Banerjee et al. [25] in Tables 3 and 4. The first four normalized mode shapes for Examples 2 and 3 are plotted in Fig. 7 for $\eta = 5$ and $\delta = 0$.

4.4 Example 4: non-rotating stepped beam

In order to show the competency of the method in determination of natural frequencies of beams with abrupt changes in cross-sectional area, a beam with one step change in cross-section is considered as shown in Fig. 8. In order to analyze this beam, each portion of the beam is considered as a single element, and the structural matrices of these two elements are finally assembled through standard finite element assemblage procedure and the free vibration analysis is

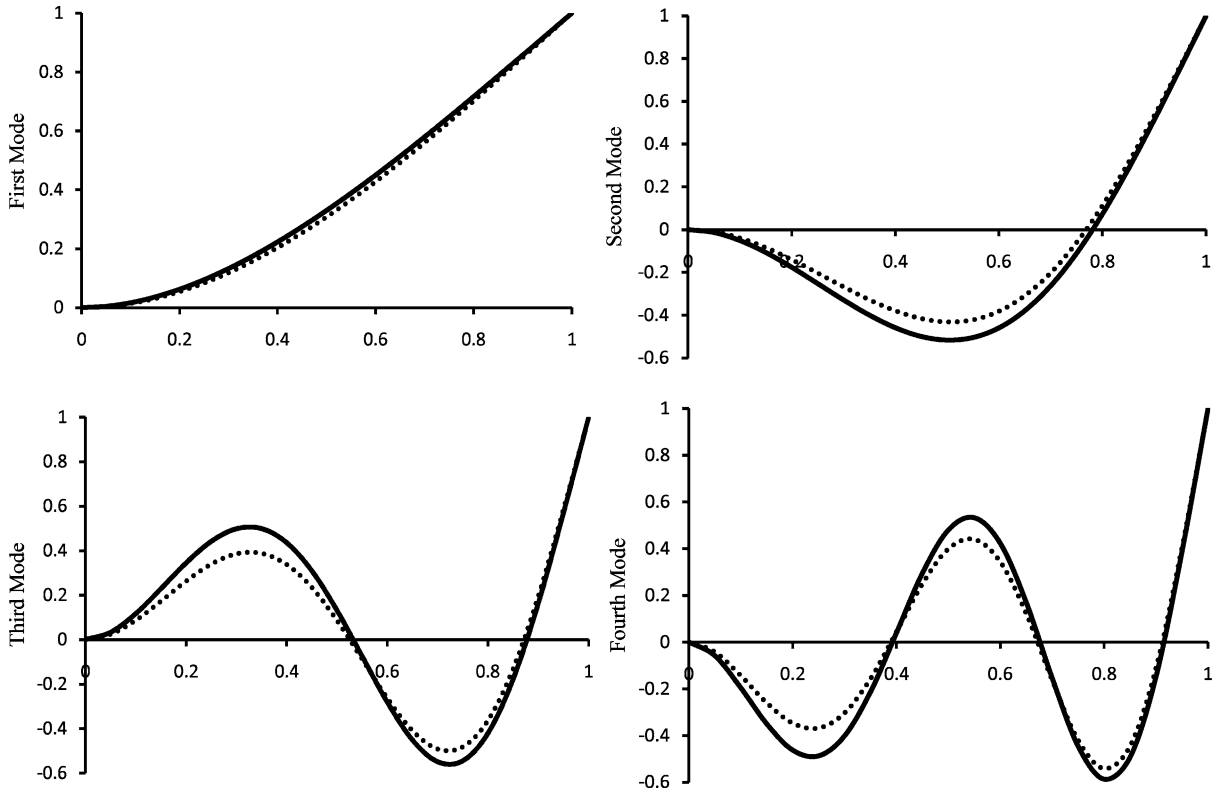

Fig. 7 The first four mode shapes of Examples 2 and 3 for $\eta = 5$ (*solid line*: Example 2, *dotted line*: Example 3)

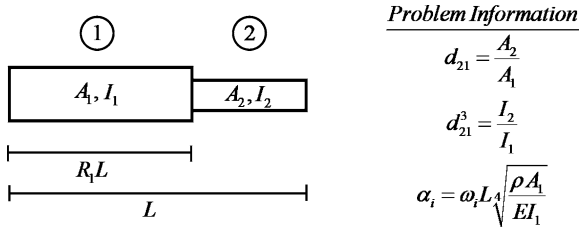

Problem Information

$$d_{21} = \frac{A_2}{A_1}$$

$$d_{21}^3 = \frac{I_2}{I_1}$$

$$\alpha_i = \omega_i L \sqrt{\frac{\rho A_1}{E I_1}}$$

Fig. 8 A beam with one step change in cross-section

carried out. The first three dimensionless natural frequencies of the beam for different boundary conditions are reported in Table 5 and compared with those of Naguleswaran [37].

5 Discussion

Through the numerical examples, it was observed that the results predicted by the proposed method are in good agreement with those in the literature. This is mostly due to the efficiency of BDFs in capturing the effects of rotational speed and variable cross-section. Figure 9 shows how BDFs vary with rotational speed parameter and taper ratio for a unit length beam element with $E = 200$ GPa, $\rho = 8000$ kg/m^3, $A_0 = 8$ cm^2, $I_0 = 60$ cm^4, $\omega = 0$, $\delta = 0$ and linearly varying height.

It is concluded from Table 1 that the natural frequencies except for the fundamental one decrease with the height taper ratio while all natural frequencies increase with breadth taper ratio. As observed in (19), the centrifugal force is proportional to the rotational speed parameter and hub radius. Moreover, centrifugal force has a stiffening effect; therefore as expected, the rotational speed parameter and hub radius have an increasing effect on the natural frequencies as introduced in Tables 2–4 and Fig. 6. In order to have a better insight, one can investigate the increasing effects of rotational speed and hub radius in Fig. 6 where it is observed that the increasing rate of all natural frequencies becomes larger for higher rotational speeds. Table 5 verifies the competency of the method in deal-

Table 5 Dimensionless natural frequencies of a non-rotating stepped beam

d_{21}	R_1		Clamped-free			Hinged-hinged			Clamped-hinged		
			$\sqrt{\alpha_1}$	$\sqrt{\alpha_2}$	$\sqrt{\alpha_3}$	$\sqrt{\alpha_1}$	$\sqrt{\alpha_2}$	$\sqrt{\alpha_3}$	$\sqrt{\alpha_1}$	$\sqrt{\alpha_2}$	$\sqrt{\alpha_3}$
0.5	0.25	Present	1.6687	3.9528	6.1635	2.2270	4.5706	7.0984	3.3603	5.6457	7.7404
		Ref. [37]	1.6687	3.9528	6.1635	2.2270	4.5706	7.0984	3.3603	5.6457	7.7404
	0.375	Present	1.8696	3.9387	6.1399	2.2637	4.9160	7.6854	3.4450	5.5281	8.1829
		Ref. [37]	1.8696	3.9387	6.1399	2.2637	4.9160	7.6854	3.4450	5.5281	8.1829
0.8	0.25	Present	1.8594	4.4137	7.2254	2.8274	5.7369	8.6953	3.7327	6.5206	9.3836
		Ref. [37]	1.8594	4.4137	7.2254	2.8274	5.7369	8.6953	3.7327	6.5206	9.3836
	0.375	Present	1.9205	4.3974	7.3419	2.8664	5.8917	8.7843	3.7177	6.5934	9.5553
		Ref. [37]	1.9205	4.3974	7.3419	2.8664	5.8917	8.7843	3.7177	6.5934	9.5553

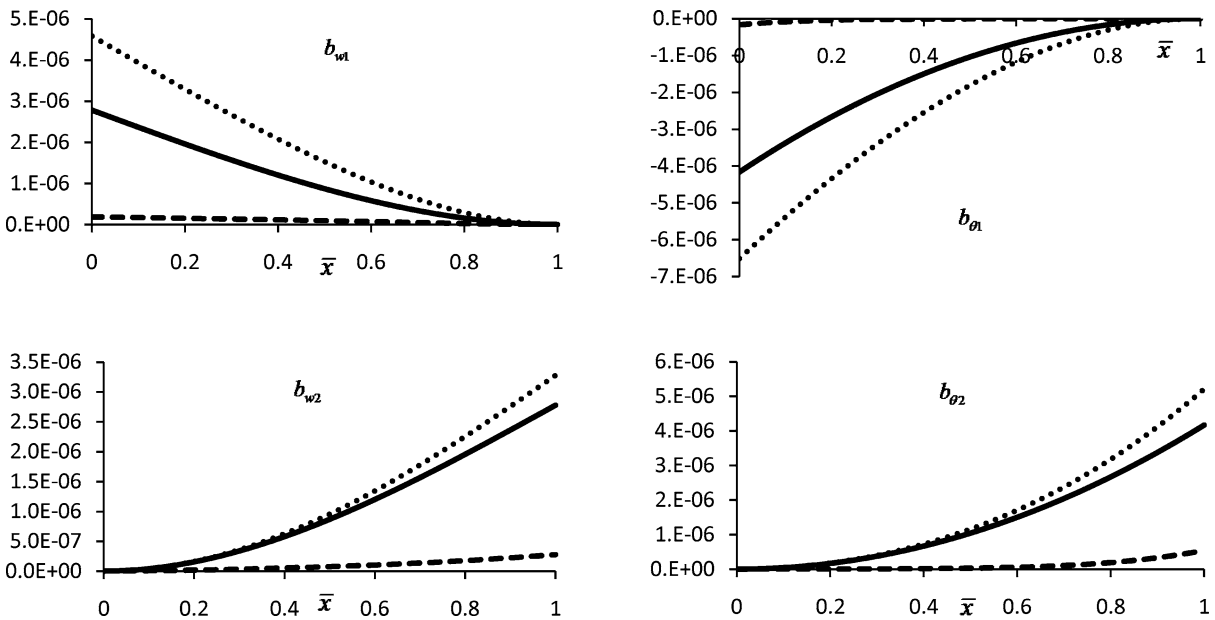

Fig. 9 Variation of BDFs with respect to rotational speed parameter and taper ratio (*solid line*: $c = 0$, $\eta = 0$, *dotted line*: $c = 0.2$, $\eta = 0$, *dashed line*: $c = 0$, $\eta = 10$)

ing with beams with discontinuity in cross-sectional profile.

In engineering applications, a new finite element could only be relied on once its convergence is studied. Here in the convergence study, the first issue which should be addressed is the accuracy of AMDM due to its direct effect on the BDFs and consequently the performance of the present element. The convergence of AMDM is guaranteed by the number of terms n used in the truncated series. In order to investigate the accuracy of AMDM, it is used directly to solve the governing differential equation for free flapwise vibration of tapered rotating beams and the natural frequencies are computed from the characteristic determinant of the system. Figure 10 depicts the convergence of AMDM with respect to n. It is observed that almost 40 terms are required so that AMDM could provide satisfactory results. The authors observed that more terms are required as the taper ratio, hub radius or rotational speed increases. The other important issue is the convergence of the method with respect to the number of elements. Using 40 terms in AMDM and consid-

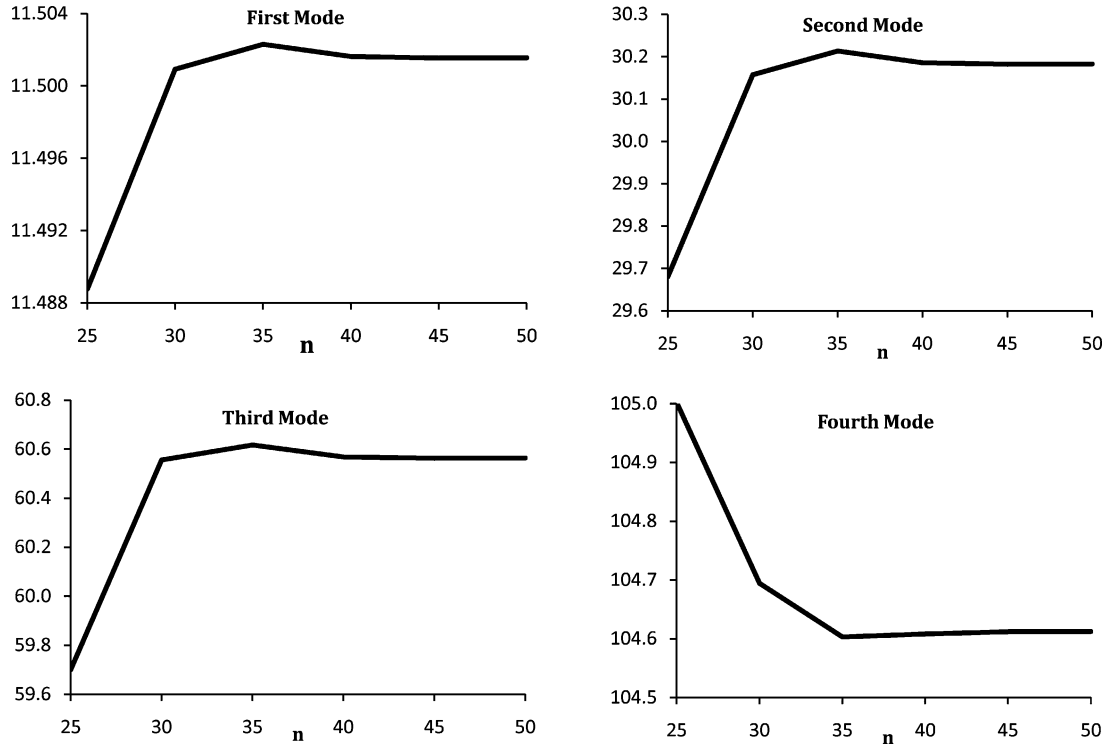

Fig. 10 Convergence of AMDM with respect to n in determination of the natural frequencies of the beam described in Example 2 under $\eta = 10$

ering the results of Banerjee et al. [25] as exact ones, the first four dimensionless natural frequencies of the beam described in Example 2 under $\eta = 10$ are determined and the relative errors are shown in Fig. 11 and compared with those of conventional finite element method (CFEM) and the beam element proposed by Bazoune [12]. It is observed that the present method provides results with high accuracy with even one element and the results change slightly with the increase in the number of elements. A very important point is deduced from Fig. 11 where we are dealing with a rotating cantilever beam. Using one beam element, there are two active degrees of freedom, degrees of freedom at the free end. As a result, the order of matrices in (34) would be 2×2 and mathematically we are able to find only the first two eigenfrequencies of the system; while Fig. 11 shows that the third and fourth natural frequencies could be also determined with employing only one element. This is possible since the new shape functions are dependent on the natural frequency ω. Consequently the value of ω affects the structural matrices and (34) would be no longer an ordinary eigenvalue problem and we are able to determine more eigenvalues than the order of the structural matrices.

6 Conclusions

Using Adomian modified decomposition method, special functions namely Basic Displacement Functions (BDFs) were obtained through solving the governing differential equation for flapwise vibration. Following basic principles of structural mechanics, the shape functions were derived in terms of BDFs. Carrying out several numerical examples, it was observed that free vibration analysis could be efficiently performed using few elements due to two facts; firstly the flexibility basis of the method brings accuracy to the results and secondly the new shape functions capture the effects of rotational speed, circular frequency, overall element configuration and physical properties. The dependency of shape functions on circular frequency enables the present element to predict many natural frequencies with only one element.

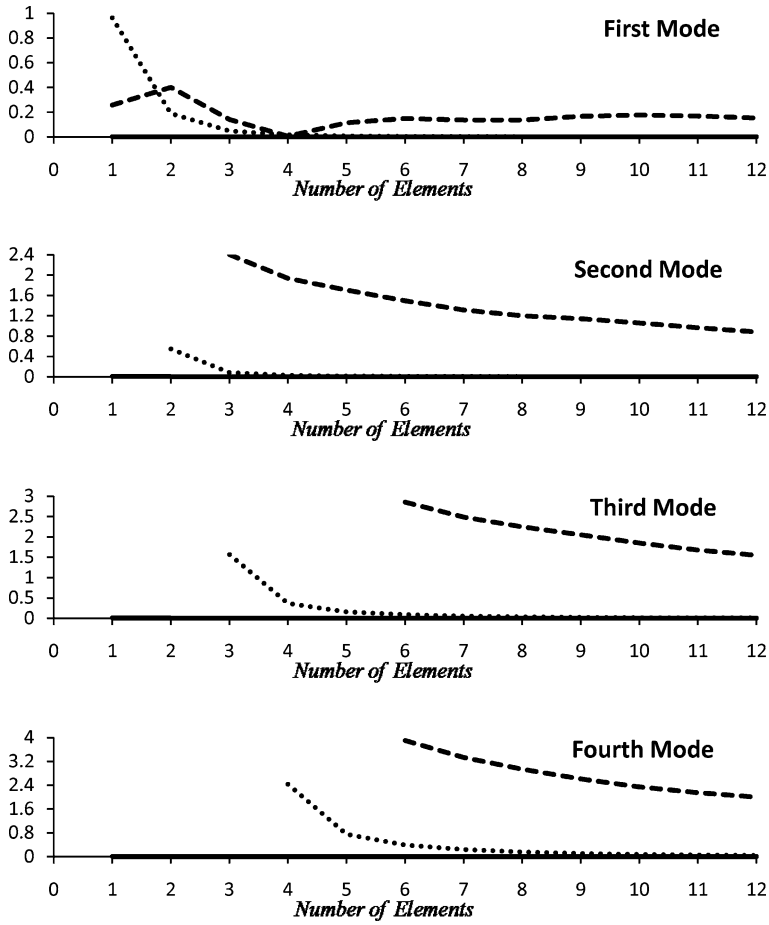

Fig. 11 Convergence of the method with respect to the number of elements (*solid line*: present; *dashed line*: CFEM; *dotted line*: element proposed by Bazoune [12])

References

1. Roy N, Ganguli R (2005) Helicopter rotor blade frequency evolution with damage growth and signal processing. J Sound Vib 283:821–851
2. Ganguli R (2001) A fuzzy logic system for ground based structural health monitoring of a helicopter rotor using modal data. J Intel Mater Syst Struct 12:397–408
3. Thakkar D, Ganguli R (2004) Helicopter vibration reduction in forward flight with induced shear based piezoceramic Actuation. Smart Mater Struct 30:599–608
4. Subrahmanyam KB, Kaza KRV (1987) Non-linear flap-lag-extensional vibrations of rotating, pretwisted, preconed beams including Coriolis effects. Int J Mech Sci 29:29–43
5. Yokoyama T (1988) Free vibration characteristics of rotating Timoshenko beams. Int J Mech Sci 30:743–755
6. Hodges DJ, Rutkowsky MJ (1981) Free vibration analysis of rotating beams by a variable order finite element method. AIAA J 19:1459–1466
7. Udupa KM, Varadan TK (1990) Hierarchical finite element method for rotating beams. J Sound Vib 138:447–56
8. Chung J, Yoo HH (2002) Dynamic analysis of rotating cantilever beam by using the finite element method. J Sound Vib 249:147–164
9. Gunda JB, Singh AP, Chhabra PS, Ganguli R (2007) Free vibration analysis of rotating tapered blades using Fourier-p superelement. Struct Eng Mech 27:243–257
10. Gunda JB, Ganguli R (2008) Stiff String basis functions for vibration analysis of high speed rotating beams. J Appl Mech 75:245021–245025
11. Shahba A, Attarnejad R, Hajilar S (2010) Free vibration and stability of axially functionally graded tapered Euler-Bernoulli beams. Shock Vib. doi:10.3233/SAV-2010-0589
12. Bazoune A (2007) Effect of tapering on natural frequencies of rotating beams. Shock Vib 14:169–179
13. Vinod KG, Gopalakrishnan S, Ganguli R (2007) Free vibration and wave propagation analysis of uniform and tapered rotating beams using spectrally formulated finite elements. Int J Solids Struct 44:5875–5893

14. Vinod KG, Gopalakrishnan S, Ganguli R (2006) Wave Propagation characteristics of rotating Euler-Bernoulli beams. Comput Model Eng Sci 16:197–208
15. Fox CHJ, Burdess JS (1979) The natural frequencies of a thin rotating cantilever with offset root. J Sound Vib 65:151–158
16. Yigit A, Scott RA, Ulsoy AG (1988) Flexural motion of a rotating beam attached to a rigid body. J Sound Vib 121:201–210
17. Wright AD, Smith GE, Thresher RW, Wang JCL (1982) Vibration modes of centrifugally stiffened beams. J Appl Mech 49:197–202
18. Wang G, Wereley NM (2004) Free vibration analysis of rotating blades with uniform tapers. AIAA J 42:2429–2437
19. Ozgumus OO, Kaya MO (2006) Flapwise bending vibration analysis of a rotating tapered cantilever Bernoulli–Euler beam by differential transform method. J Sound Vib 289:413–420
20. Ozgumus OO, Kaya MO (2006) Flapwise bending vibration analysis of double tapered rotating Euler–Bernoulli beam by using the differential transform method. Meccanica 41:661–670
21. Mei C (2008) Application of differential transformation technique to free vibration analysis of a centrifugally stiffened beam. Comput Struct 86:1280–1284
22. Attarnejad R, Shahba A (2008) Application of differential transform method in free vibration analysis of rotating non-prismatic beams. World Appl Sci J 5:441–448
23. Ozgumus OO, Kaya MO (2010) Vibration analysis of a rotating tapered Timoshenko beam using DTM. Meccanica 45:33–42
24. Banerjee JR (2000) Free vibration of centrifugally stiffened uniform and tapered beams using the dynamic stiffness method. J Sound Vib 233:857–875
25. Banerjee JR, Su H, Jackson DR (2006) Free vibration of rotating tapered beams using the dynamic stiffness method. J Sound Vib 298:1034–1054
26. Banerjee JR (2003) Free vibration of sandwich beams using the dynamic stiffness method. Comput Struct 81:1915–22
27. Gunda JB, Ganguli R (2008) New rational interpolation functions for finite element analysis of rotating beams. Int J Mech Sci 50:578–588
28. Gunda JB, Gupta RK, Ganguli R (2009) Hybrid stiff-string-polynomial basis functions for vibration analysis of high speed rotating beams. Comput Struct 87:254–265
29. Attarnejad R (2010) Basic displacement functions in analysis of non-prismatic beams. Eng Comput 27:733–745
30. Attarnejad R, Shahba A (2010) Basic displacement functions for centrifugally stiffened tapered beams. Commun Numer Methods Eng. doi:10.1002/cnm.1365
31. Attarnejad R, Shahba A (2011) Basic displacement functions in analysis of centrifugally stiffened tapered beams. Arab J Sci Eng (in press)
32. Attarnejad R, Shahba A, Jandaghi Semnani S (2011) Analysis of non-prismatic Timoshenko beams using basic displacement functions. Adv Struct Eng (in press)
33. Attarnejad R, Jandaghi Semnani S, Shahba A (2010) Basic displacement functions for free vibration analysis of non-prismatic Timoshenko beams. Finite Elem Anal Des 46:916–929
34. Adomian G (1994) Solving frontier problems of physics: the decomposition method. Kluwer Academic, Dordrecht
35. Gallagher RH, Lee CH (1970) Matrix dynamic and instability analysis with non-uniform elements. Int J Numer Methods Eng 2:265–275
36. Downs B (1977) Transverse vibrations of cantilever beam having unequal breadth and depth tapers. J Appl Mech 44:737–742
37. Naguleswaran S (2002) Natural frequencies, sensitivity and mode shape details of an Euler-Bernoulli beam with one-step change in cross-section and with ends on classical supports. J Sound Vib 252:751–767